metals

MDPI

Article

The Effect of the Bridge's Angle during Porthole Die Extrusion of Aluminum AA6082

Yu Wang * and Mary A. Wells

Mechanical and Mechatronics Engineering Department, University of Waterloo, 200 University Avenue West, Waterloo, ON N2L3G1, Canada
* Correspondence: y2275wan@uwaterloo.ca

Abstract: During the porthole die extrusion, the separated metal streams are welded together in the welding chamber. The conditions under which this occurs and the integrity of weld seam in the extrudate are impacted by the design of the bridge, including features such as its shape and dimensions. In this research, the commercial finite element method (FEM) software package, DEFORM, was used to run a series of simulation experiments in order to quantitatively understand the relationship between the bridge design and the thermal mechanical history experienced by the material during welding and the impact this has on final weld seam quality. The bridge can be roughly divided into two parts: the lower part, close to the welding chamber, and the upper part, which initially split the billet into metal streams. The results showed that increasing the lower bridge angle led to slightly higher extrusion loads and higher extrudate exit temperatures. As the lower bridge angle increased, creating a streamlined profile to a blunt profile, a dead metal zone formed under the bridge that produced higher strains near the surface of the material. In contrast, changes to the geometry of the upper bridge had little effect on the porthole die extrusion process or the thermal mechanical conditions experienced by the material.

Keywords: porthole die extrusion; bridge angle; finite element analysis; thermal mechanical history; 6xxx aluminum alloys

Citation: Wang, Y.; Wells, M.A. The Effect of the Bridge's Angle during Porthole Die Extrusion of Aluminum AA6082. *Metals* **2023**, *13*, 605. https://doi.org/10.3390/met13030605

Academic Editors: Andrzej Gontarz and Grzegorz Winiarski

Received: 21 January 2023
Revised: 28 February 2023
Accepted: 9 March 2023
Published: 16 March 2023

1. Introduction

Hollow aluminum profiles are widely used in automobile, architecture and engineering structures due to their low density, high strength and recyclability [1–3]. Among the various manufacturing techniques, porthole die extrusion is one of the most efficient, economical and flexible ways to produce hollow aluminum profiles. It is estimated that 90% of hollow aluminum profiles are manufactured using porthole die extrusion [4]. A bridge is used to support and fix the mandrel during porthole die extrusion, but the existence of bridges splits the billet into several streams. The metal streams flow around the bridges and converge under the bridges and form one or more weld seams in the extrudate. The bridge geometry greatly affects the metal flow, pressure distribution in the welding chamber and the final product's weld seam quality [5–7]. Khan et al. found the welding pressure in pointed bridge extrusion was higher than in blunt bridge extrusion [8]. Gagliardi et al. studied porthole die extrusions using three different bridge geometries, rectangle, hexagon and rhombus, and they noted that samples extruded using a rhomboidal bridge had the highest fracture strain among the three bridge geometries [6].

Rapid development of technology has led to an increased use of tools, such as commercial FEM programs as part of research programs to assist in understanding and optimizing the extrusion process. This has included aspects of the die design, material flow and final extrudate properties [9,10]. Compared to traditional "trial and error" experimental approaches for die design, the ability to perform "virtual experiments" via FEM simulation has significant advantages without the cost associated with performing numerous experiments. Research by Annadurai et al. on extrusion die design using FEM simulations led

to a reduction in experimental trials by 2/3 and a doubling of the lifespan of the die [11]. Singh et al. used HyperXtrude coupled with an optimization algorithm to reduce the speed variation at die exit from 40% to 2%; this allowed for a higher extrusion speed and less scrapped material [12]. Beyond die design, FEM simulations have shown the potential to predict extrusion defects and final extrudate microstructure, texture and mechanical properties [13,14]. Many of these FEM predictions have been verified against experimental measurements in recent research [15,16]. Wang Yu et al. used FEM model predictions to help understand the effect of the bridge shape on the textures that formed along the weld seam during porthole die extrusion [17]. The objective of this research is to use DEFORM 3D ALE (Arbitrary Lagrangian Eulerian) module to understand the relationship between the bridge die geometry (angle of the lower and upper part of the bridge) and the strain, metal flow and temperature during porthole die extrusion. This will provide the die maker with a greater quantitative understanding of these relationships and provide the necessary datasets for porthole die design predictive tools using Artificial Intelligence (AI).

Despite much research on the bridge geometry's effects on porthole die extrusion, most of the work to date has focused on two extreme cases: a pointed bridge and a blunt bridge. However, geometries between these two cases have been largely overlooked. Practice shows that a sharp streamlined bridge increases the welding quality but results in a higher maximum von Mises stress in the die and reduces the die's lifetime [8,18]. Yu et al. studied the effect of a lower bridge angle, ranging from 15° to 90°, and they believed that the preferred lower bridge angle should be the intermediate angle of 46–54°, considering both the extruded sample's mechanical properties and the die's strength [19]. In this research, a verified mathematical model of the porthole die extrusion process was used to examine the impact of changing the bridge geometry gradually from a sharp pointed tip to a blunt flat profile. This was performed so the impact of bridge sharpness on the thermal mechanical history experienced by the material and loads during extrusion could be better quantified and understood. Moreover, the design of the upper part of the bridge geometry and its effects on the porthole die extrusion have not been studied to date [18].

2. Die Design and Simulation Model

2.1. Die Design

Figure 1a shows a section view of the porthole die configuration used in this study. The die that we used produced an extrudate with a rectangular cross section and included two major parts: the die mandrel (orange) and the die plate (blue). A series of different bridge geometries were digitally created to investigate the effect of the bridge geometry (upper and lower bridge angle) on the thermal mechanical history experienced by AA6082 during porthole die extrusion. The billet was first separated into two metal streams by the bridge, and then the two streams were rejoined to each other in the welding chamber to form a longitudinal seam along the mid-width location of the extrudate. Due to the friction caused by the die wall and the bridge, the exit velocity of the material at the profile's edge compared to the middle width is relatively slower if the bearing length is uniform. Therefore, the bearing length was shorter at the edge and the middle width to balance the material's exit velocity. The extrudate was a strip with dimensions of 2.5 × 50 mm (Figure 1c) with a weld seam at the mid-width location, the billet's size was Φ106 × 200 mm and the extrusion ratio was 70.

To quantitatively understand the effect of bridge geometry on the extrusion process, the lower bridge angle was varied from 15° to 90° in increments of 15°, as shown in Figure 2. Each die configuration is designated by its lower bridge angle, such as die 15°, die 30° etc.

To investigate the influence of the upper bridge's geometry on the porthole die extrusion, three variations in terms of the geometry of the upper bridge were applied to the die with a 30° lower bridge angle and the die with a 90° lower bridge angle, as shown in Figure 3. The first variation (die 30°−1 and die 90°−1) were the same bridge shapes used to examine the lower bridge angle's effects on the extrusion, which were denoted as die 30° and die 90°, respectively. For comparison, the second and the third variation had a

sharper or blunter upper part, respectively. Table 1 summarizes the die configurations used in this research.

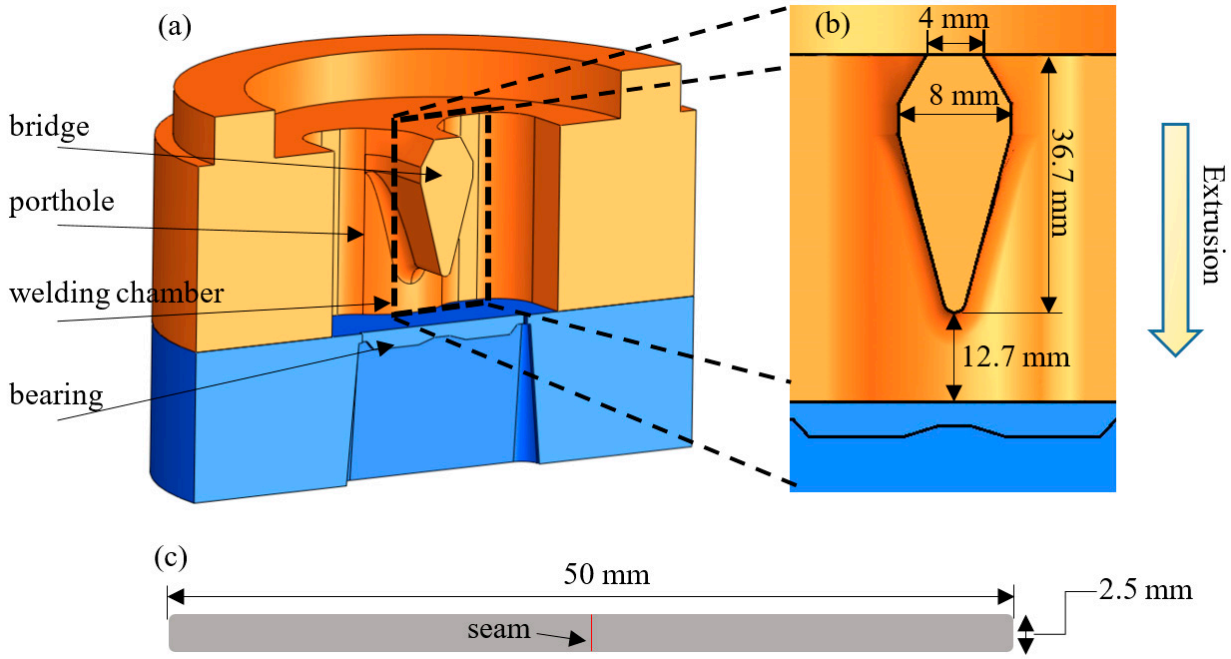

Figure 1. Schematic showing the porthole die used for this study showing: (**a**) a cut-away view of the porthole die assembly, (**b**) a cross-sectional view showing the dimensions of the die and (**c**) the cross-section of the extrudate.

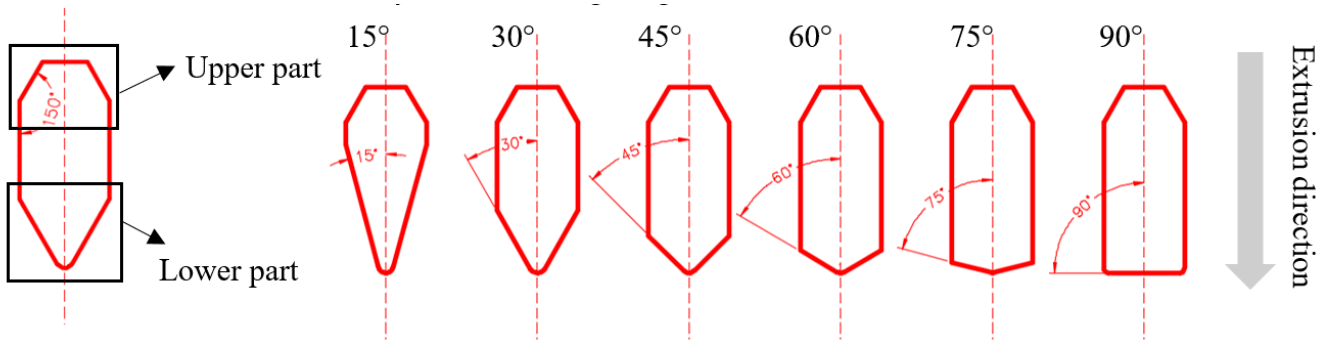

Figure 2. Series of schematics showing the range of lower bridge angles used for each simulation (far left pointed and far right blunt).

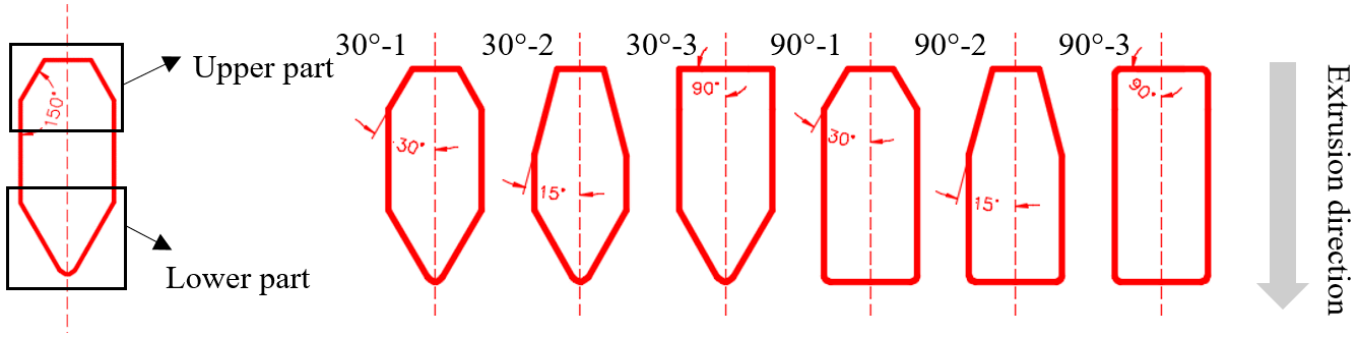

Figure 3. Schematics showing upper bridge geometries studied.

Table 1. Summary of the bridge die geometries used in this research: (a) lower bridge and (b) upper bridge.

(a)	Lower Angle	Upper Angle	(b)	Lower Angle	Upper Angle
die 15°	15°	30°	die 30°−1 (*)	30°	30°
die 30°	30°	30°	die 30°−2	30°	15°
die 45°	45°	30°	die 30°−3	30°	90°
die 60°	60°	30°	die 90°−1 (*)	90°	30°
die 75°	75°	30°	die 90°−2	90°	15°
die 90°	90°	30°	die 90°−3	90°	90°

* die 30°−1 and die 90°−1 were the same as die 30° and die 90° respectively.

2.2. Numerical Model

The simulations were carried out using an ALE module in the commercial finite element code DEFORM 3D. In the ALE simulation, the mesh nodes are neither connected to the material nor fixed in the space, but move independently from the material [20]. Compared to the Lagrangian simulation, the ALE simulation does not require frequent remeshing and can provide simulation results more precisely and efficiently.

Due to the symmetry of the die configuration, only one quarter of the billet and porthole dies were included in the model to reduce the simulation time (refer to Figure 4). All the components were meshed using tetrahedral elements, including the ram, the container and the die. In order to increase simulation efficiency without sacrificing accuracy, different parts of the billet were meshed using elements of different sizes. Since the die bearing region experienced the most severe deformation, the billet material in the die bearing region was meshed using the smallest element (0.2 mm). The material in the billet, the portholes and the welding chamber were meshed using 5 mm, 1 mm and 0.5 mm sized elements, respectively.

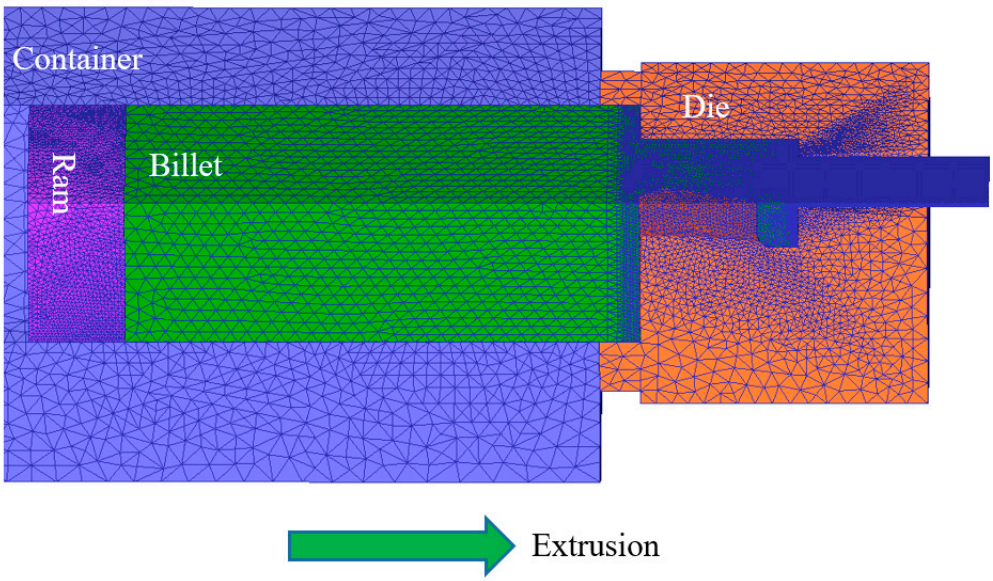

Figure 4. Schematic showing the elements and their mesh density used in each part of the ALE simulation of porthole die extrusion.

The billet and the die tooling were constructed of AA6082 and H13, respectively. Many researchers have noted that the flow stress of aluminum alloys can reach a steady value, independent of strain, at a high temperature (>0.5 Tm) [21,22]. Based on this, Sellars and Tegart proposed a hyperbolic-sine Arrhenius equation (Equation (1)) to describe

the relationship between stress, strain rate and temperature [23,24]. The hyperbolic-sine Arrhenius equation is the most widely used material model in aluminum alloy extrusion, and its effectiveness has been verified by many researchers [13,25,26]. As a result, the Sellars–Tegart model used for these simulations and its constants was determined by fitting Equation (1) to the flow stress data stored in the DEFORM database [27].

$$A[\sinh(\alpha\sigma)]^n = \dot{\varepsilon}\exp(\frac{Q_d}{RT}) \quad (1)$$

where σ is the flow stress (MPa), $\dot{\varepsilon}$ is the strain rate (s^{-1}) and T is the temperature (K). A, α, n and Q_d are material constants with value of 9.04×10^8 s^{-1}, 0.03 MPa^{-1}, 5 and 145 kJ·mol^{-1}, respectively, and R is the universal gas constant (8.314 J·mol^{-1}·K^{-1}).

The extrusion parameters used for the simulations were similar to those used during a previous extrusion trial [17]. The ram speed was 5 mm/s. The billet and the extrusion tooling temperature were 480 and 450 °C, respectively. In order to prevent the weld seam from being contaminated, no lubricant was used during the porthole extrusion trials. As a result, the billet strongly adhered to the container and die surface (except the die bearing), and the boundary condition of these interfaces were described as fully sticking without any relative velocity. On the die bearing, a shear friction model with a coefficient of 0.7 was applied [28]. Additionally, the heat transfer coefficient between the billet and the die tooling was assumed as 25 kW·$m^{-2}K^{-1}$ [29]. In the author's previous work, the validity of this model was verified by its accurate prediction of the extrusion load and the shape and size of dead metal zone; it also provided satisfactory evidence to explain the texture formation [17].

2.3. Flow Path Calculation in Post Processing

Flow path calculation is very important to analyze the material's thermal mechanical history and predict the microstructure evolution during porthole die extrusion. In this research, the flow path was calculated based on the velocity field obtained from the ALE simulation. The algebra and verification of the flow path calculation was illustrated in detail in the author's previous work [17]. Figure 5 shows the flow path (purple line) of a tracked point from a mid-thickness location along the weld line of the extruded strip during porthole die extrusion performed with a lower bridge angle of 15°. Since the tracked point was exactly on the weld seam at a mid-thickness location of the extruded strip, the thermal mechanical history of this point represents the thermal mechanical history of the seam. The tracked point experienced four stages during porthole die extrusion: splitting, porthole, welding chamber and exit [4]. During the splitting stage, the billet was divided into two metal streams by the bridge. In the porthole, the tracked point flowed on the surface of the bridge and accumulated a significant amount of strain under the friction shear stresses. These separated metal streams rejoined each other in the welding chamber and formed the weld seam in the middle of the profile. Finally, the material was squeezed out of the die to form the desired extrudate. In this paper, the state variables and thermal mechanical history in each stage were carefully examined in order to understand the effect of the bridge geometry on the porthole die extrusion.

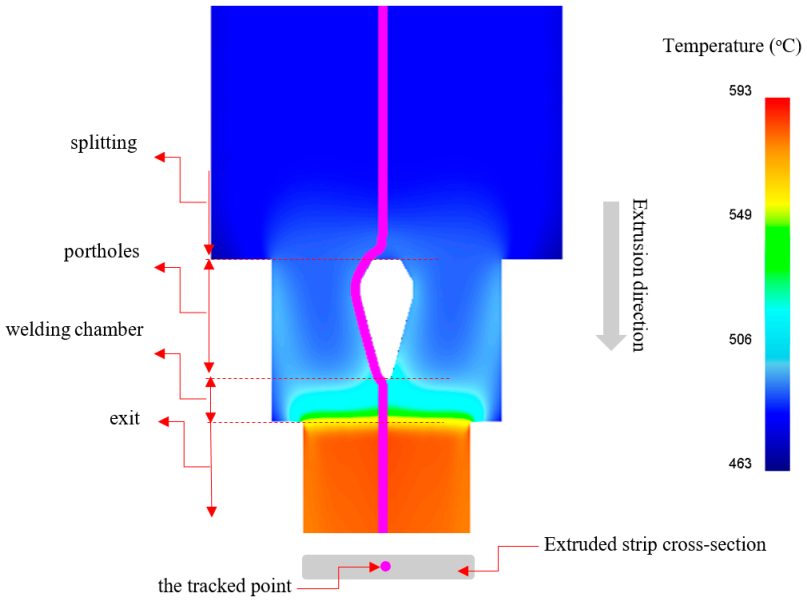

Figure 5. Schematic showing a cross-sectional view of the porthole die extrusion process indicating the flow path of the weld seam material at different stages in the process.

3. Results and Discussion

3.1. Design of Lower Bridge

3.1.1. Extrusion Load

The prediction of the extrusion load using FEM simulation is very important to the extrusion industry. On one hand, the predicted extrusion load is something measured in practice and can be used to verify the validity of the FEM model. On the other hand, it helps industry to select the appropriate extrusion machine with sufficient capacity [16,30]. Figure 6 shows the model-predicted extrusion load for different lower bridge angles at the breakthrough when the ram speed and extrusion temperature were 5 mm/s and 480 °C, respectively. The extrusion load increased slightly by 2.6% (~14 tons) as the lower bridge angle increased. According to Gagliardi et al. [18], the extrusion load increases with the bridge volume due to its larger obstruction. In this case, the volume of the bridge increased with the lower bridge angle, ranging from 1.4×10^4 mm^3 to 2.0×10^4 mm^3 as the lower bridge angle increased from 15° to 90°.

3.1.2. Velocity Distribution

Figure 7 showed the model-predicted effect of the lower bridge angle on the velocity field in the welding chamber during porthole die extrusion. When the lower bridge angle was varied from 15° to 45°, the velocity beneath the bridge maintained a high speed over 30 mm/s, except for a very thin layer of the material that was stuck to the surface of the bridge (Figure 7a–c). When the lower bridge angle was 60°, there existed a small part of the material under the bridge, that had a flow speed less than 3 mm/s. As the lower bridge angle continued to increase, a dead metal zone formed, and this expanded significantly under the bridge. When the bridge angle reached 75° and 90°, the dead metal zone was so large that it could not be neglected (circled in Figure 7e,f). The presence of a dead metal zone under the bridge can disrupt the smoothness of the material's flow.

The velocity differences around the bridge for different bridge angles affect the time needed for the weld seam material (the tracked point shown in Figure 5) to pass through the porthole and welding chamber, as shown in Table 2. When the lower bridge angle was 15°, it took only 0.31 s for the weld seam material to pass though the welding chamber. On the other hand, when a dead metal zone exists, the weld seam material stayed in the welding chamber for 3.0 s when the lower bridge angle was 90°; this is ten times longer

than with the die with a 15° angle. As the lower bridge angle increases, the weld seam material is in the porthole region for a longer time too. As the lower bridge angle increased from 15° to 90°, the time needed to pass through the porthole stage increased from 4.3 to 9.5 s.

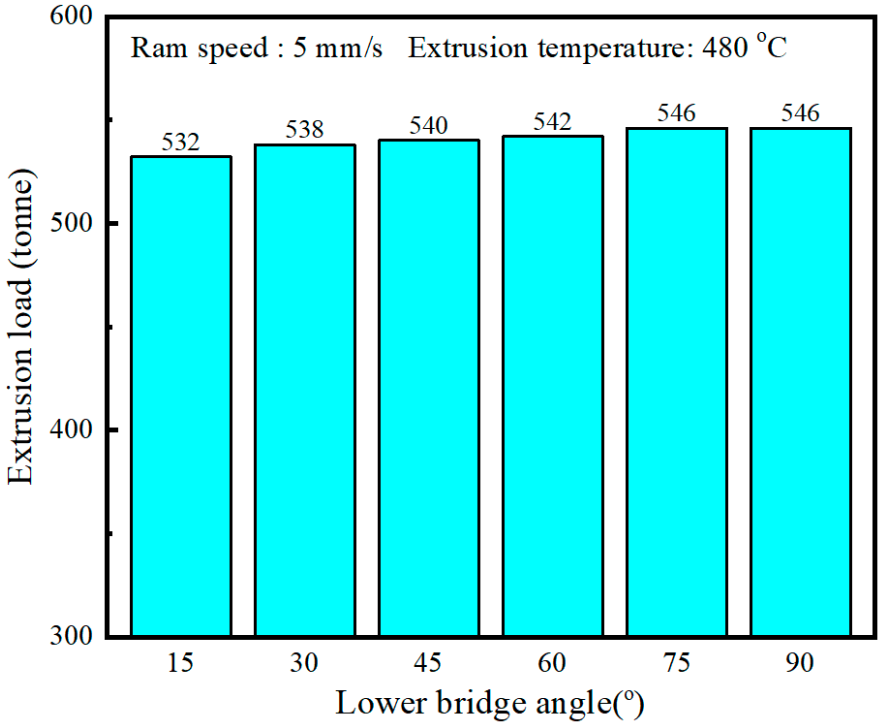

Figure 6. Model-predicted extrusion load versus lower bridge angle.

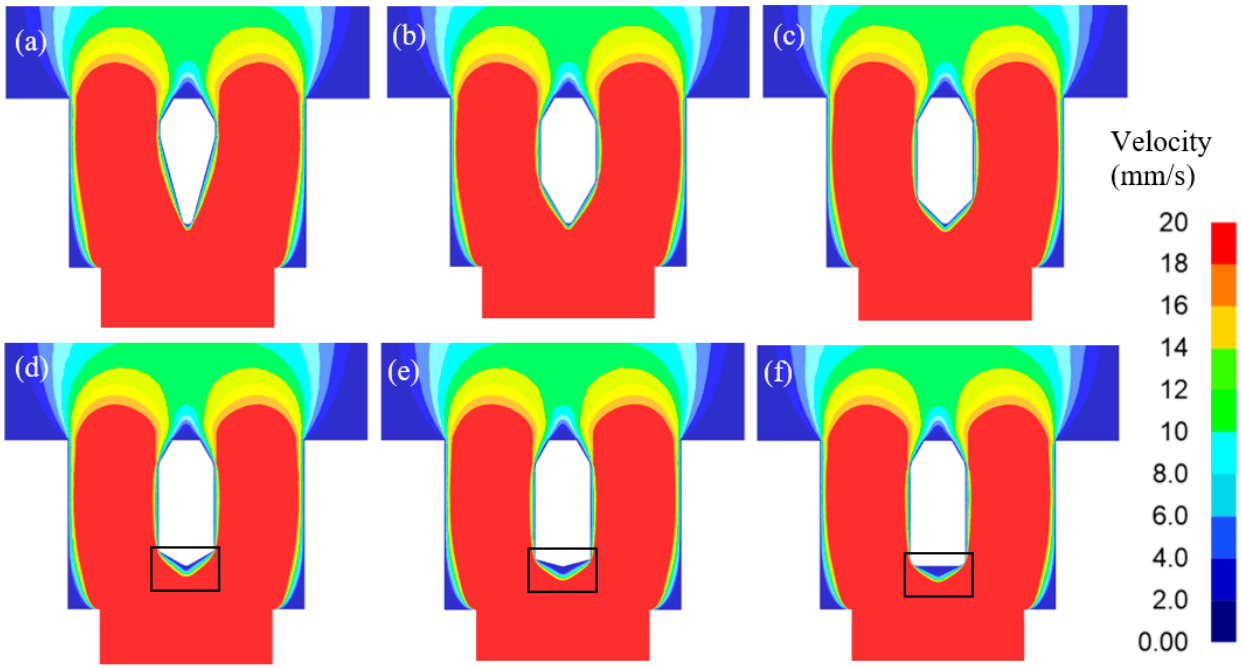

Figure 7. Cross-sectional view of the model-predicted velocity distribution in the welding chamber for different lower bridge angles: (**a**) 15°, (**b**) 30°, (**c**) 45°, (**d**) 60°, (**e**) 75° and (**f**) 90°.

Table 2. The time needed for the seam material to pass through the porthole and welding stage.

Lower Bridge Angle	15°	30°	45°	60°	75°	90°
Porthole (s)	4.3	4.9	4.9	5.8	8.0	9.5
Welding chamber (s)	0.31	0.33	0.44	0.67	1.4	3.0

3.1.3. Temperature Distribution

Figure 8 showed the model-predicted temperature distribution through the cross-section of the extruded profile at the die exit. Since the welding region (the middle of the extrudate) experienced the most severe deformation, it always had a relatively higher temperature than the material around it. Moreover, the temperature of the welding region also increased as the lower bridge angle increased. For instance, the die with a 90° angle had the highest temperature (583 °C) at the weld region, while the weld seam temperature produced using the die with a 15° angle was lowest (579 °C). The profile's surface temperature showed the same trend, and it also increased with the lower bridge angle (Figure 9). To quantitatively show the temperature differences between different lower bridge angles, the model-predicted temperature distribution across the extrudate at a mid-thickness location (the black line shown in Figure 8) was plotted in Figure 10. As shown in Figure 11, the weld seam's temperature was about 4.5 °C higher for the extrusion performed with a lower bridge angle of 90° when compared to an extrusion performed for a lower bridge angle of 15°. Though 4.5 °C did not seem to be a significant temperature difference, the experimental result showed that the die with a 90° lower bridge angle produced an extruded profile with a very rough surface close to the weld seam [31]. The weld seam temperature for the bridges with the smaller lower bridge angles could be because of the smoother material flow and absence of the dead metal zone. The impact of the smaller lower bridge angles on the temperature diminished as we move away from the weld seam. As shown in Figure 11, the model-predicted exit temperature of a region 12 mm away from the weld seam was only 1.4 °C higher when extruded using a die with a lower bridge angle of 90° when compared to a die with a lower bridge angle of 15°.

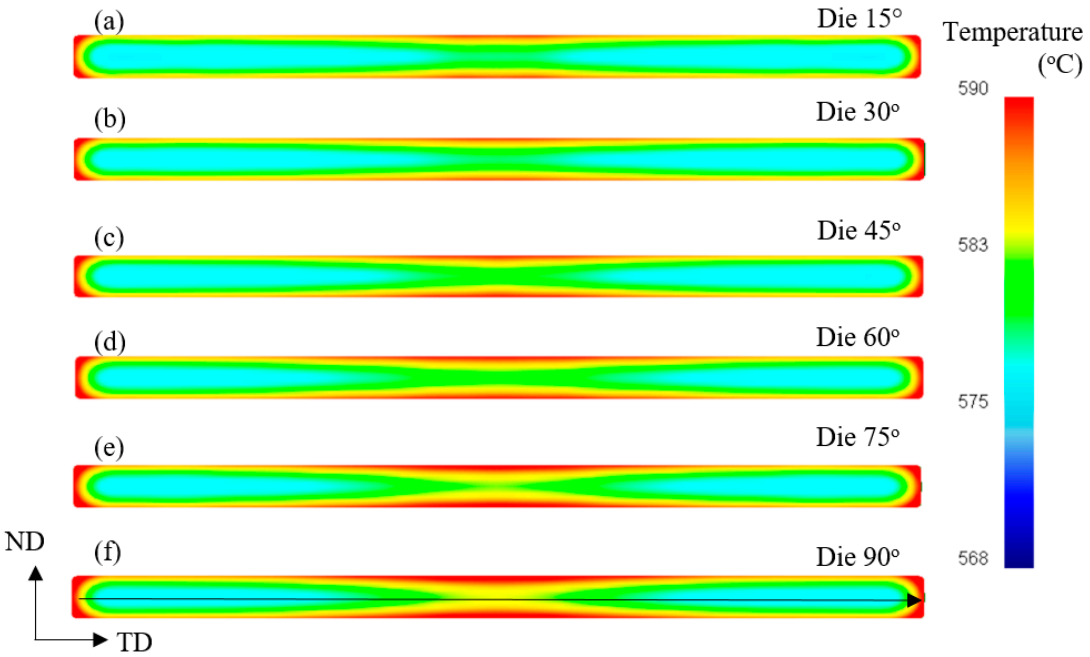

Figure 8. Cross-sectional view of the model-predicted extrudate's exit temperature during porthole die extrusion for lower bridge angles of: (**a**) die 15°, (**b**) die 30°, (**c**) die 45°, (**d**) die 60°. (**e**) die 75° and (**f**) die 90°.

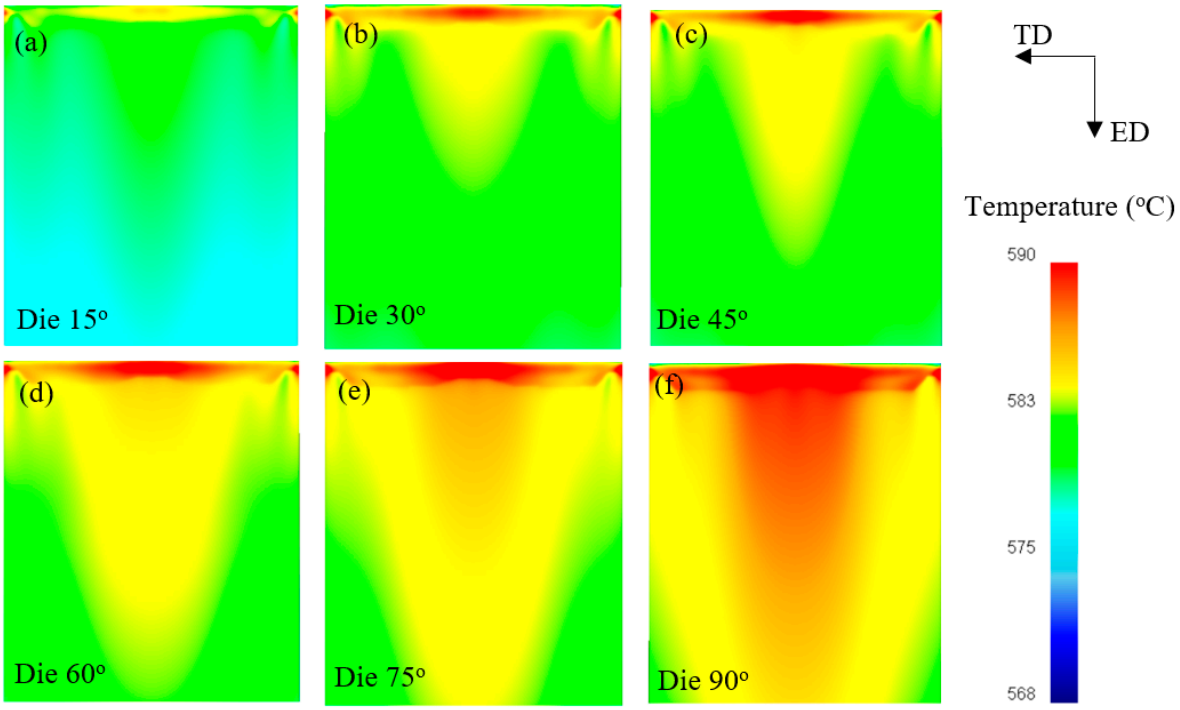

Figure 9. Model-predicted surface temperature distribution of the extrudate's surface just after the die exit of porthole extrusions made using varying lower bridge angles: (**a**) die 15°, (**b**) die 30°, (**c**) die 45°, (**d**) die 60°. (**e**) die 75° and (**f**) die 90°.

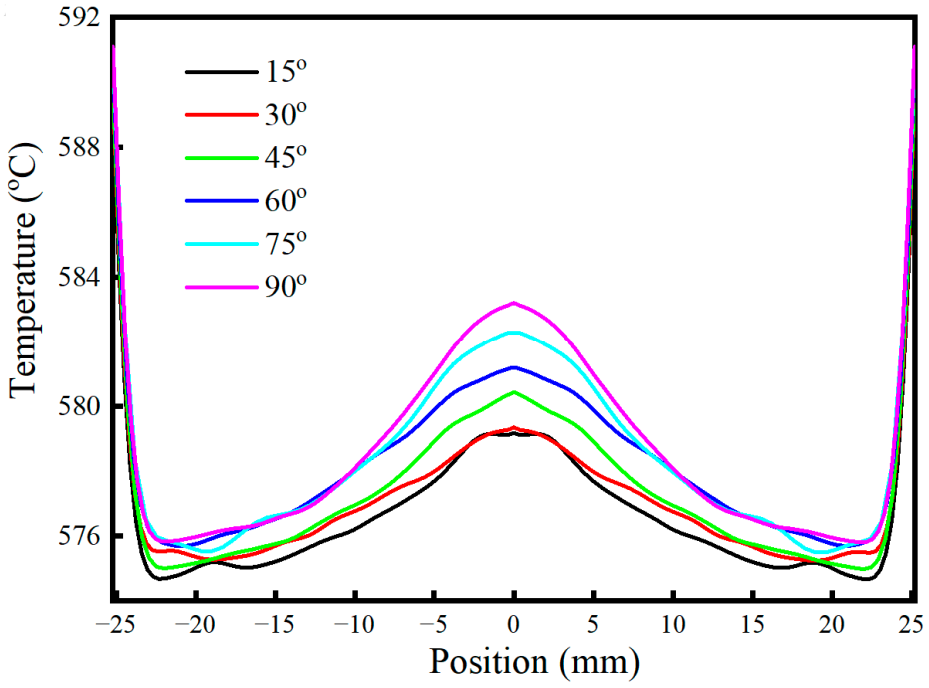

Figure 10. Effect of lower bridge angle on the model-predicted exit temperature across the extrudate at a mid-thickness location (the black line in Figure 8f).

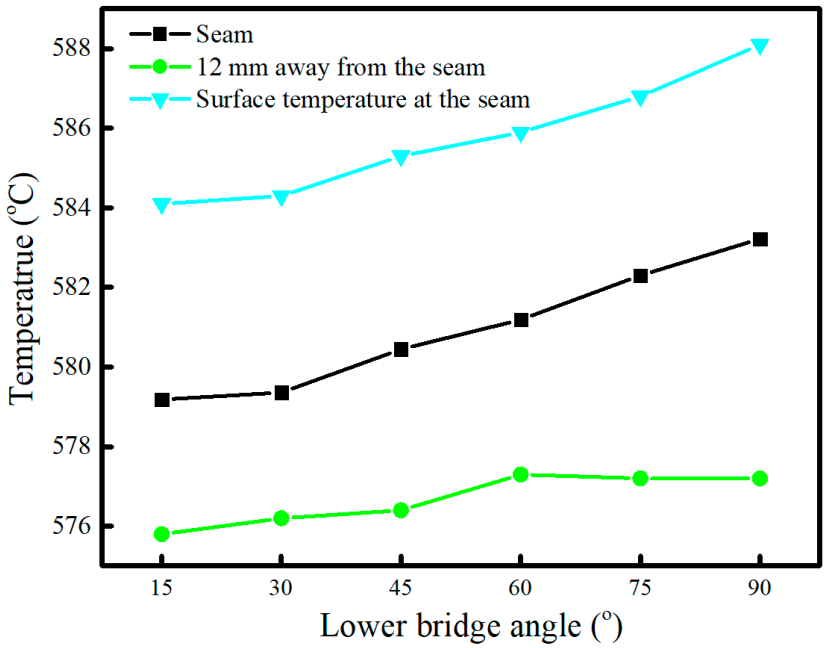

Figure 11. Effect of lower bridge angle on the model-predicted temperature of the extrudate at a mid-thickness location for the weld seam (black), 12 mm away from the weld seam (green) and the surface temperature above the weld seam (blue).

3.1.4. Strain Distribution

The accumulated plastic strain was calculated by integration of the effective strain rate over time along the flow path, as shown in Equation (2).

$$\varepsilon = \oint \dot{\varepsilon}_{effective} \mathrm{d}t \tag{2}$$

Figure 12 showed the model-predicted evolution of strain across the extrudate as the lower bridge angle was varied from 15° to 90°. Referring to Figure 12a, when the lower bridge angle was 15°, the red high strain region at the seam was lenticular shaped with a very slight bulge at the mid-thickness. As the lower bridge angle was increased to 45°, the bulge of the high strain region grew slightly larger into the neighboring material (Figure 12b,c). When the lower bridge angle was 60°, the bulge of the high strain region at the mid-thickness was obvious. As the lower bridge angle was further increased to 90°, the high strain region at the mid-thickness location of the weld seam had grown and extended the furthest into the neighboring material. This corresponds to experimental work conducted by Wang et al. that also showed that the weld seam transformed from linear to cross shape as the lower bridge angle increased [19]. The velocity distribution (Figure 7) showed the material flow became less smooth and even obstructed by the dead metal zone in the welding chamber as the lower bridge angle increased. As a result, a higher strain accumulated at the weld seam region and more material close to the weld seam was affected due to the increasing of the lower bridge angle. Figure 13 shows the strain distribution along the mid-thickness (red line in Figure 12f) of the extrudate profile from the weld seam to the strip edge. At a location about 4 mm away from the seam, the strain in all the extrusions with different lower bridge angles converge at 5.2. As a comparison, the strain of the sample extruded without a bridge was about 5.0 at the die exit. This shows that the influence of the bridge diminishes away from the seam. These results are supported by experimental work [31] that showed that, for lower bridge angles of 30°, the bridge only affected the material's texture about 1 mm away from the bridge; meanwhile, for material extruded using a lower bridge angle of 90°, the bridge influenced the material's texture as far as 3 mm away from the weld seam.

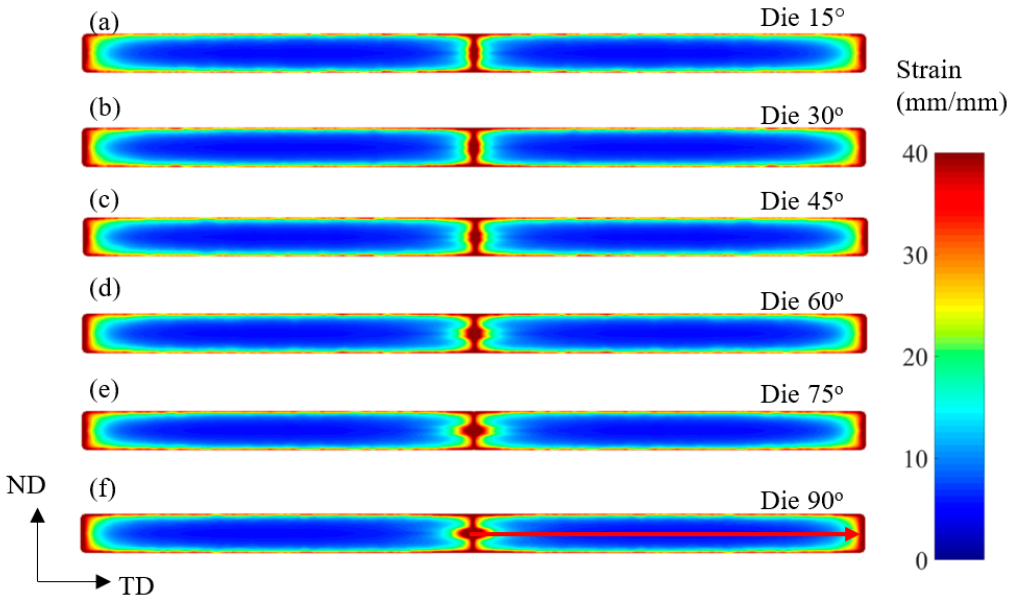

Figure 12. Cross-sectional view of the effect of the lower bridge angle on the model-predicted strain across the extrudate: (**a**) die 15°, (**b**) die 30°, (**c**) die 45°, (**d**) die 60°. (**e**) die 75° and (**f**) die 90°.

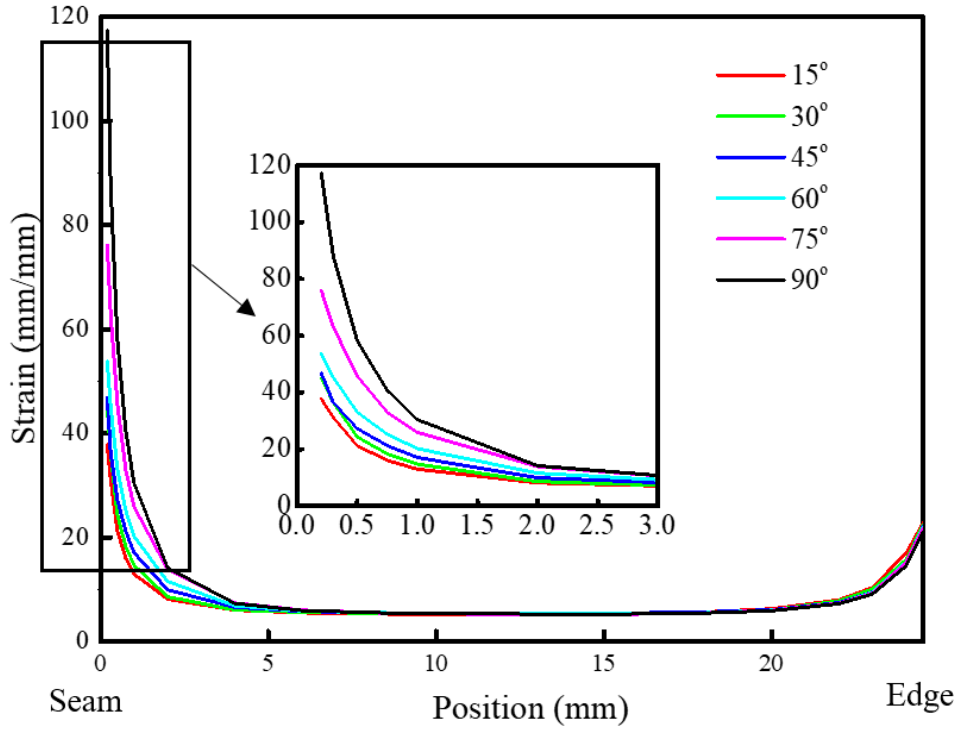

Figure 13. Model-predicted strain distribution showing the effect of lower bridge angle on the strain along the seam to the edge of the extrudate at the mid-thickness location (the red line in Figure 12f).

Figure 14 showed the strain at the weld seam versus the lower bridge angle. When the lower bridge angle ranged from 15° to 45°, the strain value (around 40) of the weld seam was almost unchanged. However, when the lower bridge angle was greater than 60°, the strain at the weld seam increased very sharply as the lower bridge angle increased due to the formation and obstruction of the dead metal zone under the bridge. During extrusion with a lower bridge angle of 90°, the strain of the welding region can be as high as 117.

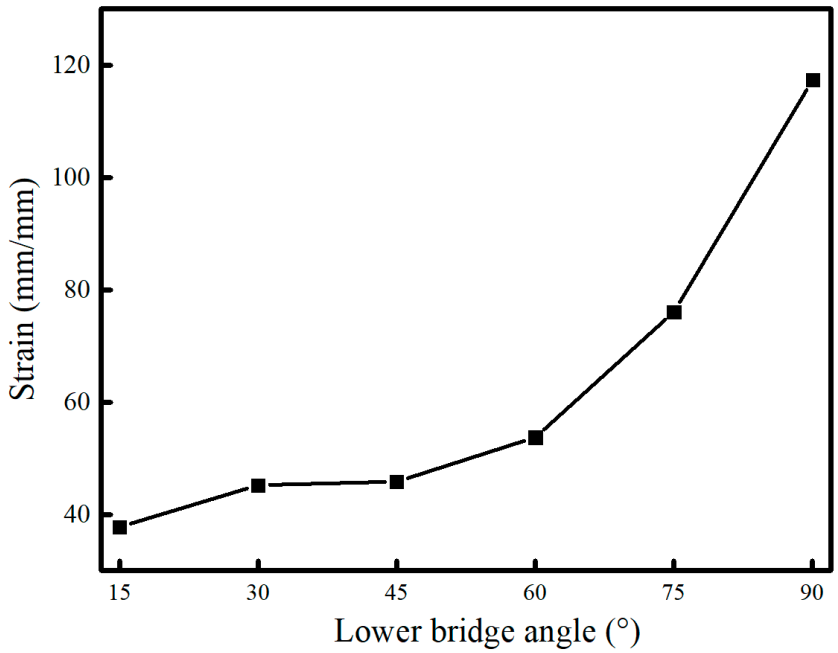

Figure 14. Model-predicted effect of lower bridge angle on the strain at the mid-thickness of weld seam after extrusion.

3.1.5. Thermal Mechanical History

Thermal mechanical history is very important in determining the microstructure and texture of the extrudate. In this research, each points' state variables on the flow path were obtained using an interpolation method. The thermal mechanical history was obtained by relating the point's state variables and their corresponding time. In this paper, the time when the material exited the die was denoted as 0 s.

Figure 15 shows the model-predicted thermal history of the weld seam material using different lower bridge angles during extrusion. As mentioned earlier, the porthole die extrusion can be roughly divided into four stages: splitting, porthole, welding chamber and exit. Examining the thermal history of the weld seam material (the tracked point shown in Figure 5) during extrusion using a lower bridge angle of 90°, the temperature began to rise from the billet temperature of 480 °C when the splitting occurs at around 17 s (noted by the splitting arrow in Figure 15). After the material (see Figure 5) entered the portholes at around 12.5 s, its temperature increased because of the strong friction shear stress from the bridge surface; however, it also lost some heat due to its contact with the cold bridge. As a result, the temperature increased slowly during this stage. In the welding chamber, the temperature saw the largest increase, from 510 to 590 °C, due to the severe plastic deformation it experienced. Weld seam material extruded using lower bridge angles experienced very similar thermal histories, but each stage happened at different times due to their different velocities. For instance, the splitting stage of material extruded using a lower bridge die 15° occurred at 7 s (noted by a red arrow in Figure 15), and the temperature also began to rise at the same time.

Figure 16 shows the effective strain history of the weld seam material for different bridge angles. As with thermal history, the strain history can also be roughly divided into four stages. Examining the strain history of the weld seam extruded using a lower bridge angle of 90°, we see the strain began to increase when the splitting stage occurred at 17 s. When the weld seam entered the porthole at around 12.5 s, the effective strain was already ~7 due to the deformation that occurred at the splitting stage. In the porthole stage, the flow path on the surface of the bridge experienced a very high strain rate due to friction, so the strain value increased from 7 to 105. Finally, in the welding chamber, the strain value continued to rise 105 to 120 at the exit. Material extruded using other lower bridge angles

experienced a similar pattern of strain accumulation. However, similar to the thermal history, the strain and the time of each stage were very different depending on the lower bridge angle.

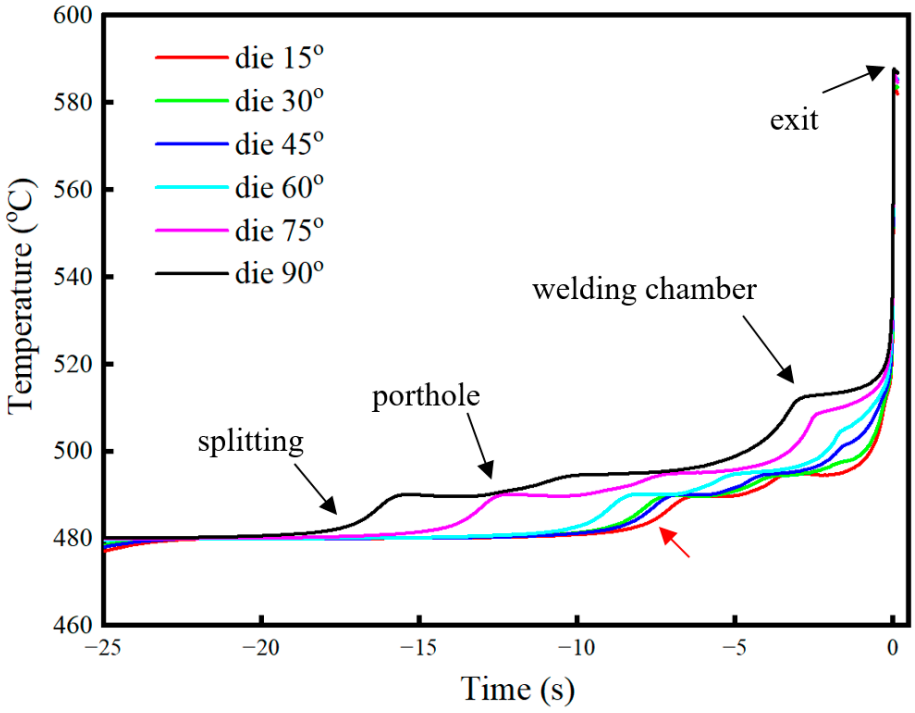

Figure 15. Model-predicted thermal history at the weld seam (mid-thickness) showing the effect of lower bridge angle.

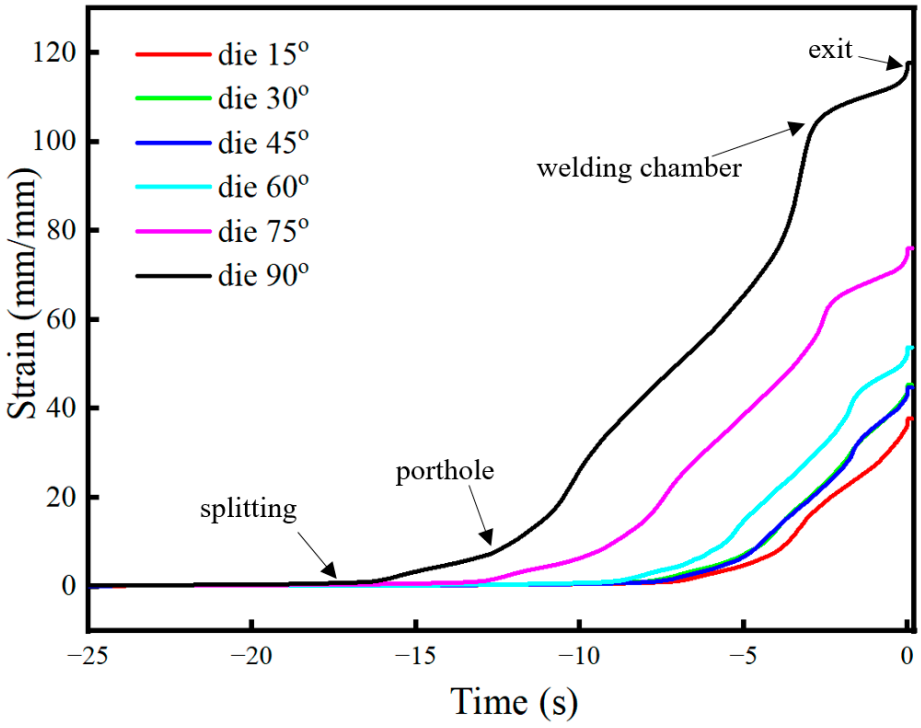

Figure 16. Model-predicted strain history at the mid-thickness of the weld seam for different lower bridge angles in the extrusion process.

3.1.6. Weld Quality

Currently, there are three widely accepted criteria used to predict the welding quality of the weld seam. One of them is the "Q-criterion", proposed by Plata and Piwnik [32], based on the assumption that a strong bond is formed once the deformation energy is above a critical value. The disadvantage of the "Q-criterion" is that it gives an unreasonably high value of the deformation energy if the material is stuck in the dead metal zone for a long period of time. In order to solve this problem, Donati and Tomesani [33,34] proposed the "K-criterion" by taking the velocity into consideration. In their research, the "K-criterion" proved to be better than the "Q-criterion" at predicting weld quality of AA6084 alloy porthole die extrusion [33]. In recent years, Yu et al. [14,35] suggested that sufficient strain is necessary to break the contaminant and expose clear material to form a sound weld. Therefore, the strain was expressed as the integral of strain rate over time in their proposed "J-criterion" (Equation (3)). According to their study on the porthole die extrusion of complex profiles, the "J-criterion" gave the most accurate prediction among the three [14]. In this research, the "J-criterion" was used to compare the weld quality of profiles extruded using different lower bridge angles.

$$J = \int_0^t k_0 \frac{\sigma_m}{\overline{\sigma}} \dot{\overline{\varepsilon}} \exp\left(\frac{RT}{Q_D}\right) \mathrm{d}t \tag{3}$$

where k_0 is the coefficient related to the material and surface condition for bonding (assumed to be 1 in this study), σ_m is the mean stress normal stress (MPa), $\overline{\sigma}$ is the effective stress (MPa), $\dot{\overline{\varepsilon}}$ is the effective strain rate (s^{-1}), R is the universal gas constant (8.314 $J \cdot mol^{-1} \cdot K^{-1}$), T is the absolute temperature (K), Q_d is the diffusion activation energy (which is 1.45×10^5 $J \cdot mol^{-1}$ from 450 to 650 °C [14]) and t is the time (s).

Table 3 shows the "J criterion" parameters when the lower bridge angle varied from 15° to 90°. The welding quality was very similar when the lower bridge angle was smaller than 45°. However, the welding quality parameter began to drop as the lower bridge angle increased beyond 60°. In porthole die extrusion design, the welding quality parameter should always be above a critical value to achieve a sound weld. Sound weld quality means the weld seam does not contain voids and its strength is equivalent to the matrix. In research by Yu et al. [14], the critical "J value" for AA 6084 alloy to achieve a sound welding quality is 10.8; this is below all of the J values of the die configurations examined in this paper (Table 3). Despite the different welding parameters using different lower bridge angles, it seems that all of them can achieve a satisfactory weld quality based on this criterion. This simulation result also agreed with the author's experimental results: that the die 30° and die 90° extruded samples had almost the same strength and elongation [36].

Table 3. The predicted weld quality of porthole die extrusion using different lower bridge angles.

Weld Quality Parameter	Die 15°	Die 30°	Die 45°	Die 60°	Die 75°	Die 90°
J	15.4	15.1	15.8	14.7	13.7	13.4

3.2. Design of Upper Bridge

3.2.1. Temperature Distribution

Figure 17 shows the model-predicted temperature distribution at the die exit when the geometry of the upper bridge was varied for dies with a lower bridge angle of 30° and 90° during extrusion. A change in geometry of the upper bridge did not have a significant effect on the temperature distribution. As shown in Figure 18, the temperature difference between die 90°−1 and die 90°−2 was only about 0.7 °C along the weld line. On the other hand, the temperature difference between die 30°−1 and die 90°−1 was about 4.5 °C along the weld line. It is very clear that the exit temperature is much more sensitive to the geometry of the lower bridge but not the geometry of the upper bridge.

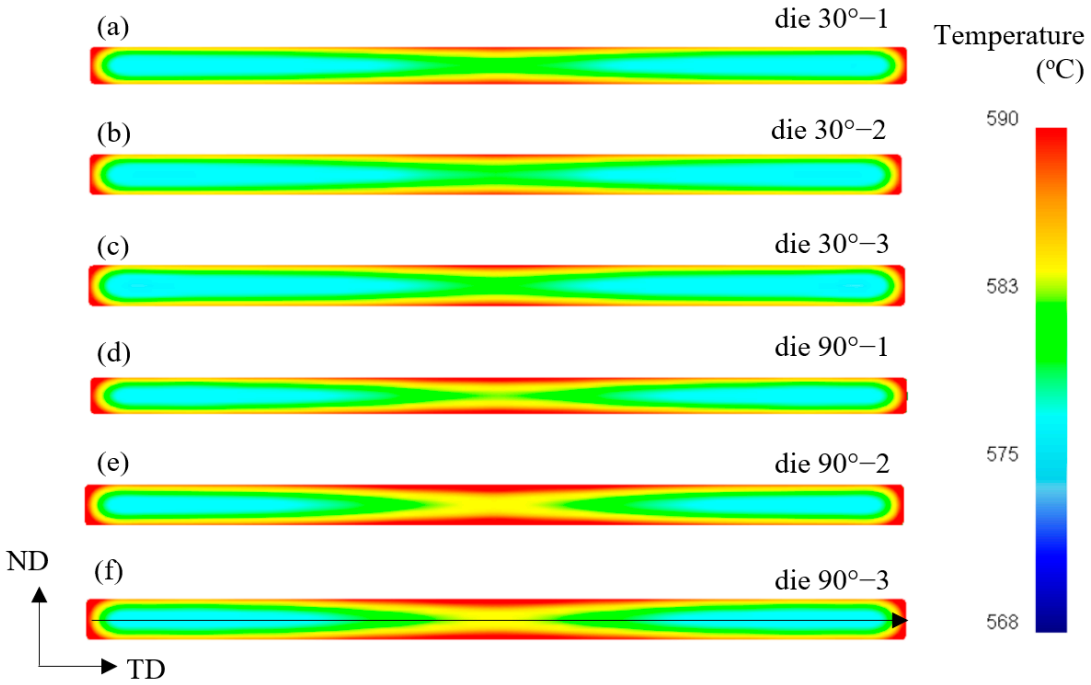

Figure 17. Model-predicted cross-sectional view of the extrudate's exit temperature showing the effect of the upper bridge's geometry: (**a**) die 30°−1, (**b**) die 30°−2, (**c**) die 30°−3, (**d**) die 90°−1. (**e**) die 90°−2 and (**f**) die 90°−3.

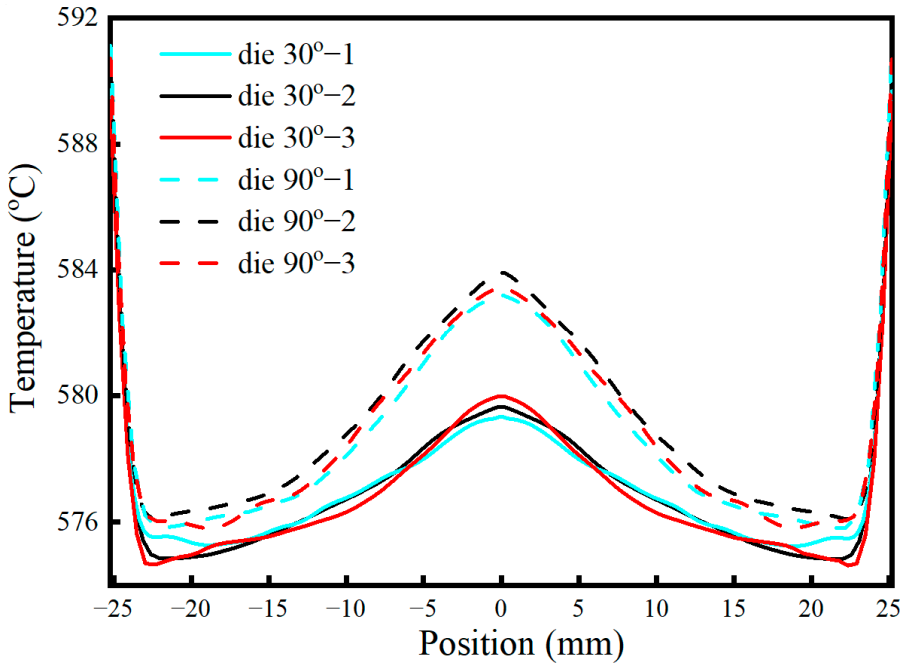

Figure 18. Model predicted exit temperature distribution of the extrudate along the middle thickness (the black line in Figure 17f) and how it is affected by the upper geometry.

3.2.2. Strain Distribution

Figure 19 shows the model-predicted strain distribution through the cross section of the extrudate using different upper bridge geometries. In a very similar way to the effect of the upper bridge's shape on temperature distribution, there was very little effect of this on the strain distribution in the extrudate.

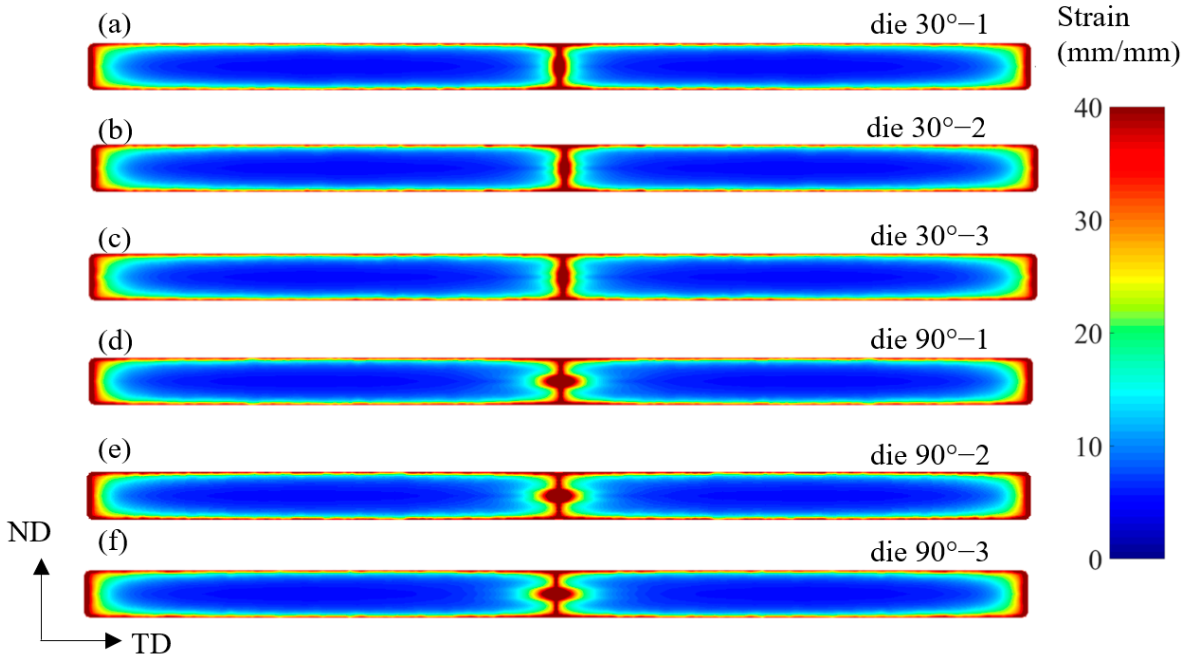

Figure 19. Strain distribution at the die exit of the profiles extruded using bridges with different upper bridge's geometries. (**a**) die 30°−1, (**b**) die 30°−2, (**c**) die 30°−3, (**d**) die 90°−1. (**e**) die 90°−2 and (**f**) die 90°−3.

Based on the above discussion, it is safe to say that the shape of the upper part of the bridge has a negligible influence on the temperature and strain distribution of the extrusion near the weld line relative to the effect of the geometry of the lower part of the bridge.

3.2.3. Strain History

Figure 20 shows the effective strain history of the weld seam's material for different upper bridge's geometries. The upper bridge angle of 30° and 15° had almost the same strain history, but the upper bridge angle of 90° had a slightly higher strain. The blunt upper part of the bridge had more difficulties in splitting the billet into two metal streams when compared with the other two smaller upper bridge angles; as such, it accumulated more strain during the splitting stage. For dies with a lower angle of 30°, the strain value in the bridge with the upper bridge angle of 90° (die 30°−3) was about 7.5 at the end of the splitting stage (marked by the red arrow in Figure 20a). Meanwhile, the strain value in the upper bridge angle of 30° (die 30°−1) and 15° (die 30°−2) was about 5.8 at the end of the splitting stage (marked by the black arrow in Figure 20a). Similarly, die 90°−3 with the upper bridge angle of 90° also showed a higher strain (≈13) at the end of the splitting (marked by the red arrow in Figure 20b) compared with the strain (≈7) in die 90°−1 (30° upper bridge angle) and die 90°−2 (15° upper bridge angle) when the splitting finished (marked by the black arrow in Figure 20b). Despite the blunt upper part of the bridge resulting in a slightly higher strain from the splitting, the strain difference between the three variations was still very small when compared to the total strain. Compared to the impact of the lower bridge angle, the upper die geometry has a much smaller impact on the strain history of the weld seam.

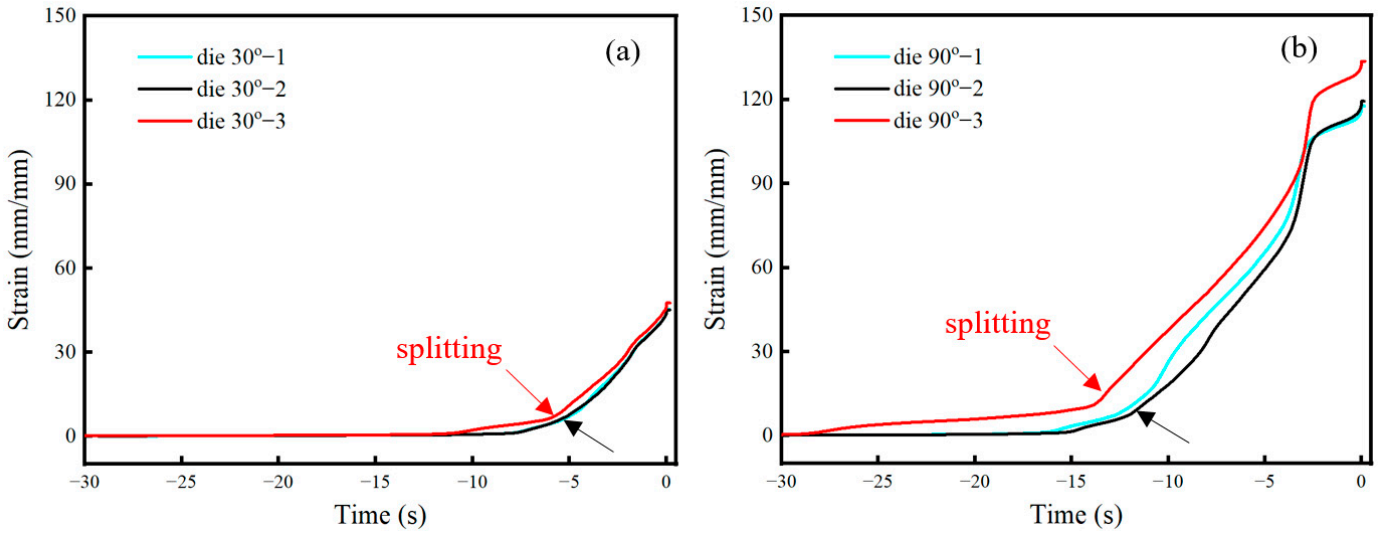

Figure 20. Model predicted strain history of the weld seam material and how it is impacted by the upper bridge's geometry: (**a**) die 30° series and (**b**) die 90° series.

4. Conclusions

A verified DEFORM 3D ALE module was applied to predict the exit temperature, strain and the thermal mechanical history of the porthole die extrusions using varying bridge geometries. The purpose of this research was to obtain a quantitative understanding on the role of bridge geometry design on the final extrudate and quality of the welds produced. This information can help die makers design bridges for different extrudates and qualitatively assess the impact on microstructure. From this research, the following conclusions can be drawn:

1. The velocity distribution in the welding chamber and the material flow was directly influenced by the lower bridge angle. When the lower bridge angle was above 60°, a dead metal zone began to form under the bridge and disrupted the material flow.
2. As the lower bridge angle increased from 15° to 90°, the temperature of the welding seam increased from 579 °C to 583 °C and the strain increased from 40 to 117. The strain distribution plot implies that the microstructure and texture of the weld seam and its adjacent areas can be influenced by the geometry of the lower part of the bridge, but the rest of the material was almost unaffected.
3. The upper part of the bridge only affected the splitting stage of the porthole die extrusion, but its overall influence on the porthole die extrusion and final extrudate was negligible compared by the lower part of the bridge.

Author Contributions: Conceptualization, Y.W. and M.A.W.; methodology, Y.W.; software, Y.W.; validation, Y.W.; formal analysis, Y.W.; investigation, Y.W.; resources, M.A.W.; data curation, Y.W.; writing—original draft preparation, Y.W.; writing—review and editing, Y.W. and M.A.W.; visualization, Y.W.; supervision, M.A.W.; project administration, M.A.W.; funding acquisition, M.A.W. All authors have read and agreed to the published version of the manuscript.

Funding: The funding has come from Natural Sciences and Engineering Research Council of Canada (NSERC) tri-council both from an alliance grant and discovery grant.

Institutional Review Board Statement: Not applicable.

Informed Consent Statement: Not applicable.

Data Availability Statement: The raw/processed data required to reproduce these findings cannot be shared at this time as the data also forms part of an ongoing study. However, the data used to support the findings of this study may be made available from the corresponding author upon request.

Acknowledgments: This work was undertaken, in part, thanks to the guidance of Warren, J. Poole from the University of British Columbia, support of Nick, C. Parson from Rio Tinto Aluminium, Mei Li form the Ford Motor Company and the financial support from the NSERC is gratefully acknowledged.

Conflicts of Interest: The authors declare no conflict of interest.

References

1. Chen, H.; Zhao, G.Q.; Zhang, C.S.; Guan, Y.J.; Liu, H.; Kou, F.J. Numerical simulation of extrusion process and die structure optimization for a complex aluminum multicavity wallboard of high-speed train. *Mater. Manuf. Process.* **2012**, *26*, 1530–1538. [CrossRef]
2. Liu, P.; Xie, S.; Cheng, L. Die structure optimization for a large, multi-cavity aluminum profile using numerical simulation and experiments. *Mater. Des.* **2012**, *36*, 152–160. [CrossRef]
3. Fang, W.; Tang, D.; Wang, H.; Li, D.; Peng, Y. Optimization of die design for thin-walled flat multi-port tube with the aid of finite element simulation. *J. Mater. Process. Technol.* **2020**, *277*, 116418. [CrossRef]
4. Liu, G.; Zhou, J.; Duszczyk, J. FE analysis of metal flow and weld seam formation in a porthole die during the extrusion of a magnesium alloy into a square tube and the effect of ram speed on weld strength. *J. Mater. Process. Technol.* **2008**, *200*, 185–198. [CrossRef]
5. Valberg, H. Extrusion welding in aluminium extrusion. *Int. J. Mater. Prod. Technol.* **2002**, *17*, 497–556. [CrossRef]
6. Gagliardi, F.; Ambrogio, G.; Filice, L. On the die design in AA6082 porthole extrusion. *Cirp Ann.-Manuf. Technol.* **2012**, *61*, 231–234. [CrossRef]
7. Khan, Y.A.; Valberg, H.; Irgens, I. Joining of metal streams in extrusion welding. *Int. J. Mater. Form.* **2009**, *2*, 109–112. [CrossRef]
8. Khan, Y.A.; Valberg, H.S.; Jacobsen, B.O.T. Deformation conditions in the extrusion weld zone when using pointed and square ended bridge. *Int. J. Mater. Form.* **2010**, *3*, 379–382. [CrossRef]
9. Liu, Y.; Xu, J.; Zhang, Z.; Liu, G.; Shan, D.; Zhang, L.; Guo, B. Micro-extrusion process and microstructure evolution of miniature heat pipe in 6063 aluminum alloy. *Int. J. Adv. Manuf. Technol.* **2022**, *120*, 6463–6480. [CrossRef]
10. Wang, Y.; Zhao, G.; Zhang, W.; Sun, L.; Wang, X.; Lv, Z. Interfacial bonding mechanism and length evaluation method of the longitudinal welds in the unsteady deformation process of porthole die extrusion of aluminum alloy profiles. *J. Mater. Res. Technol.* **2022**, *20*, 1624–1644. [CrossRef]
11. Annadurai, S.; Mulla, I.; Mohammed, M. Die Correction and Die Design Enhancement using Profile Simulation in Extrusion Industry. In Proceedings of the Twelfth International Aluminum Extrusion Technology Seminar and Exposition, Orlando, FL, USA, 3–5 May 2022.
12. Singh, N.; Singh, G.; Skinner, J.; Ravisankar, M. Bearing Profile and Shape Optimization of an Industrial Hollow Profile Die. In Proceedings of the Twelfth International Aluminum Extrusion Technology Seminar and Exposition, Orlando, FL, USA, 3–5 May 2022.
13. Kolpak, F.; Schulze, A.; Dahnke, C.; Tekkaya, A.E. Predicting weld-quality in direct hot extrusion of aluminium chips. *J. Mater. Process. Technol.* **2019**, *274*, 116294. [CrossRef]
14. Yu, J.; Zhao, G.; Cui, W.; Chen, L.; Chen, X. Evaluating the welding quality of longitudinal welds in a hollow profile manufactured by porthole die extrusion: Experiments and simulation. *J. Manuf. Process.* **2019**, *38*, 502–515. [CrossRef]
15. Manik, T.; Marthinsen, K.; Zhang, K.; Aria, A.I.; Holmedal, B. Deformation Texture Evolution in Flat Profile AlMgSi Extrusions: Experiments, FEM, and Crystal Plasticity Modeling. *Front. Mater.* **2021**, *8*, 636379. [CrossRef]
16. Wang, Y.; Zhao, G.; Chen, X.; Xu, X. Cracking behavior and prediction criterion of spray-deposited 2195 Al–Li alloy extrusion profile. *Int. J. Adv. Manuf. Technol.* **2022**, *120*, 5969–5984. [CrossRef]
17. Wang, Y.; Zang, A.; Mahmoodkhani, Y.; Wells, M.; Poole, W.; Parson, N. The Effect of Bridge Geometry on Microstructure and Texture Evolution During Porthole Die Extrusion of an Al–Mg–Si–Mn–Cr Alloy. *Metall. Mater. Trans. A* **2021**, *52*, 3503–3516. [CrossRef]
18. Gagliardi, F.; Schwane, M.; Citrea, T.; Haase, M.; Khalifa, N.B.; Tekkaya, A.E. Bridge design influences on the pressure conditions in the welding chamber for porthole die extrusion. *Key Eng. Mater.* **2014**, *622–623*, 87–94. [CrossRef]
19. Wang, Y.; Zhao, G.; Sun, L.; Wang, X.; Wei, D.; Liu, L. Effects of welding angle on microstructure and mechanical properties of longitudinal weld in 6063 aluminum alloy extrusion profiles. *J. Mater. Res. Technol.* **2022**, *17*, 756–773. [CrossRef]
20. Zhang, C.; Zhao, G.; Chen, Z.; Chen, H.; Kou, F. Effect of extrusion stem speed on extrusion process for a hollow aluminum profile. *Mater. Sci. Eng. B* **2012**, *177*, 1691–1697. [CrossRef]
21. Lin, Y.C.; Chen, X.-M. A critical review of experimental results and constitutive descriptions for metals and alloys in hot working. *Mater. Des.* **2011**, *32*, 1733–1759. [CrossRef]
22. Dong, Y.; Zhang, C.; Zhao, G.; Guan, Y.; Gao, A.; Sun, W. Constitutive equation and processing maps of an Al-Mg-Si aluminum alloy: Determination and application in simulating extrusion process of complex profiles. *Mater. Des.* **2016**, *92*, 983–997. [CrossRef]
23. Sellars, C.; Tegart, W.M. Hot workability. *Int. Metall. Rev.* **1972**, *17*, 1–24. [CrossRef]
24. Sheppard, T.; Wright, D.S. Determination of flow stress: Part 1 constitutive equation for aluminium alloys at elevated temperatures. *Met. Technol.* **1979**, *6*, 215–223. [CrossRef]

25. Zhang, K.; Marthinsen, K.; Holmedal, B.; Aukrust, T.; Segatori, A. Through thickness variations of deformation texture in round profile extrusions of 6063-type aluminium alloy: Experiments, FEM and crystal plasticity modelling. *Mater. Sci. Eng. A* **2018**, *722*, 20–29. [CrossRef]
26. Tang, D.; Zhang, Q.; Li, D.; Peng, Y. A physical simulation of longitudinal seam welding in micro channel tube extrusion. *J. Mater. Process. Technol.* **2014**, *214*, 2777–2783. [CrossRef]
27. Mahmoodkhani, Y.; Chen, J.; Wells, M.A.; Poole, W.J.; Parson, N.C. The Effect of Die Bearing Geometry on Surface Recrystallization During Extrusion of an Al-Mg-Si-Mn Alloy. *Metall. Mater. Trans. A* **2019**, *50*, 5324–5335. [CrossRef]
28. Jowett, C.; Mahmoodkhani, Y.; Parson, N.C.; Garza, G. What Does Exit Temperature Measurement Tell Us. In Proceedings of the Eleventh International Aluminum Extrusion Technology Seminar and Exposition, Chicago, IL, USA, 2–6 May 2016.
29. Duan, X.; Sheppard, T. Simulation and control of microstructure evolution during hot extrusion of hard aluminium alloys. *Metall. Mater. Trans. A* **2003**, *351*, 282–292. [CrossRef]
30. Donati, L.; Tomesani, L. The effect of die design on the production and seam weld quality of extruded aluminum profiles. *J. Mater. Process. Technol.* **2005**, *164–165*, 1025–1031. [CrossRef]
31. Wang, Y. Effect of Bridge Geometry on Seam Weld Microstructures in AA6xxx Aluminum Porthole Die Extrusions. Ph.D. Thesis, University of Waterloo, Waterloo, ON, Canada, 2020.
32. Plata, M.; Piwnik, J. Theoretical and experimental analysis of seam weld formation in hot extrusion of aluminum alloys. In Proceedings of the Seventh International Aluminum Extrusion Technology Seminar, Chicago, IL, USA, 16–19 May 2000.
33. Donati, L.; Tomesani, L. The prediction of seam welds quality in aluminum extrusion. *J. Mater. Process. Technol.* **2004**, *153-154*, 366–373. [CrossRef]
34. Donati, L.; Tomesani, L. Seam welds in hollow profile extrusion: Process mechanics and product properties. *Mater. Sci. Forum* **2009**, *604*, 121–131. [CrossRef]
35. Yu, J.; Zhao, G.; Chen, L. Analysis of longitudinal weld seam defects and investigation of solid-state bonding criteria in porthole die extrusion process of aluminum alloy profiles. *J. Mater. Process. Technol.* **2016**, *237*, 31–47. [CrossRef]
36. Wang, Y.; Zang, A.; Mahmoodkhani, Y.; Parson, N.C.; Wells, M.A.; Poole, W.J.; Li, M. The Effect of Bridge Geometry during Porthole Extrusion on the Mechanical Properties of 6xxx-Series Alloys. In Proceedings of the Twelfth International Aluminum Extrusion Technology Seminar and Exposition, Orlando, FL, USA, 3–5 May 2022.